ISSN 0031-918X, Physics of Metals and Metallography, 2021, Vol. 122, No. 9, pp. 883–890. © © The Author(s), 2021. This article is an open access publication.
Russian Text © The Author(s), 2021, published in Fizika Metallov i Metallovedenie, 2021, Vol. 122, No. 9, pp. 948–956.

STRUCTURE, PHASE TRANSFORMATIONS, AND DIFFUSION

The Effect of Heat Treatment on the Structure and Mechanical Properties of Nanocrystalline Cu–14Al–3Ni Alloy Subjected to High-Pressure Torsion

A. E. Svirid[a, *], V. G. Pushin[a, b], N. N. Kuranova[a, b], V. V. Makarov[a], and A. N. Uksusnikov[a]

[a] *Institute of Metal Physics, Ural Branch, Russian Academy of Sciences, Ekaterinburg, 620990 Russia*

[b] *Ural Federal University Named after the First President of Russia B.N. Yeltsin, Institute of Natural Sciences and Mathematics, Ekaterinburg, 620002 Russia*

**e-mail: svirid2491@rambler.ru*

Received March 24, 2021; revised May 14, 2021; accepted May 18, 2021

Abstract—The effect of heat treatment on the microstructure, phase composition, mechanical properties, and microhardness of the shape-memory Cu–14 wt % Al–3 wt % Ni alloy prepared in the nanocrystalline state, which results from the severe plastic high-pressure torsion (HPT), is studied. Electron microscopy and X-ray diffraction analysis are used in combination with electrical resistivity measurements in order to obtain data on the peculiarities of thermoelastic martensitic transformations and decomposition in the HPT-processed alloy subjected to thermal actions.

Keywords: copper alloy, severe plastic deformation by torsion, heat treatment, thermoelastic martensitic transformation, shape-memory effect, mechanical properties

DOI: 10.1134/S0031918X21090131

INTRODUCTION

The application of thermal actions, mechanical loadings, and magnetic fields in order to ensure thermoelastic martensitic transformations (TMT) in various alloys allows a wide range of crucial physical phenomena to be realized. Single and iterative reversible shape-memory effects (SME), giant superelasticity, and giant elasto-, magnetocaloric, and damping effects are among the phenomena that separate so-called intellectual or smart materials to in a specific individual class of practically important structural polyfunctioning materials [1–5]. At the current stage of development of engineering and technology, there is a need for such smart materials, which can be used under different temperature, force, and other practically important conditions, in particular, in a large-size state. At the same time, the low plasticity and brittleness of these materials, except binary titanium nickelides, do not allow these unique effects to be realized for the polycrystalline state. Because of these, tasks of the optimum alloying and development of methods and technologies for plasticization of different polycrystalline SME materials in order to ensure their many-sided industrial applications become increasingly important, but unresolved in practice.

Copper β alloys, such as Cu–Al–Ni, Cu–Zn–Al, and Cu–Zn–Sn are characterized by the lower cost, better thermal and electrical conductivity, and workability, as compared to those of, for example, titanium nickelides [3–6]. Moreover, these alloys in the single-crystal state demonstrate excellent SME characteristics. In the case of the common coarse-grained (CG) polycrystalline state, these alloys are characterized by very low plasticity, fracture strength, and fatigue life [1, 3, 6]. This fact does not allow the SME inherent for single crystals to be realized.

The specific cause for the intercrystalline fracture is the high anisotropy of elastic constants, $A = C_{44}/C'$ (12–13 units), of copper alloys that are metastable with respect to TMT [7], which is 1–2 for elastically isotropic plastic titanium nickelides with low elastic constants [4, 5]. The high elastic anisotropy upon TMT leads to substantial elastic stresses at junctions of martensite packets and, in particular, at grain boundaries; the coarser the alloy grains, the higher the value of stresses and their localization at boundaries. The chemical segregation and heterogeneous decomposition in these coarse-grained alloys aggravate the decrease in the plasticity, first of all, at temperatures below the eutectoid decomposition boundary (T_{ed}) close to 840 K [3]. It is obvious that the intercrystalline brittleness is one of the key causes that impede the application of SME alloys in practice. The weakening in the role of the above factors in the embrittlement of copper SME alloys is possible at the expense of the radical decrease in the grain size during severe plastic

deformation (SPD) and, therefore, the increase in the boundary length [8–14]. At the same time, other various methods used for refining the grain structure of the alloys [15–21] with application of alloying additions [17, 21], heat treatment [15–18], rapid quenching [6], powder metallurgy and others [19, 20], as a rule, were found to be ineffective.

The aim of this study is to investigate the effect of heat treatment on the grain size, structural and phase transformations, mechanical properties, and hardness of the SMA Cu–14Al–3Ni alloy subjected to SPD.

EXPERIMENTAL

The alloy having a nominal composition of Cu–14 wt % Al–3 wt % Ni (from herein, the Cu–14Al–3Ni alloy) was melted using high purity Cu, Al, and Ni (99.99% purity), subjected to hot forging at 1173–1273 K to form a rod 20 × 20 mm in section, and water quenching from 1223 K after 10-min holding. A number of samples were also subjected to repeated water quenching from 1273 K after heating for 30 min. To refine the grain structure, the SPD by torsion under a high pressure of 6 MPa was used. It was realized at room temperature in flat heads with a "groove" (cylindrical hollow in the bottom head) using 1, 5, and 10 revolutions and at 423 K using 10 revolutions. Samples for the HPT were prepared in the form of disks 20 mm in diameter and 1.2 mm in thickness. The value of their true deformation (e) at the midradius of sample subjected to HPT with 10 revolutions was 6.0. Isochronous isothermal annealings of HPT-processed samples were performed at in a temperature range of 373–873 K (at a step of 100 K) for 30 min. Moreover, the short-term of the subjected to HPT was performed at 1073 K for 10 s. The TMT temperatures were determined during cyclic temperature measurements of the electrical resistivity $\rho(T)$ at heating and cooling rates of 5 K/min. The structure and phase composition of the alloy subjected to deformation at room temperature and subsequent annealings were studied by X-ray diffraction (XRD) analysis, transmission and scanning electron microscopy (TEM and SEM, respectively) using back-scattered electron diffraction (BSED) mode. The XRD analysis was performed using monochromatized Cu $K\alpha$ radiation. The following equipment available at the Center of the Collaborative Access, Institute of Metal Physics, Ural Branch, Russian Academy of Sciences was used: a Tecnai G^2 30 transmission electron microscope (operating at an accelerating voltage of 300 kV) and a Quanta 200 scanning electron microscope (operating at an accelerating voltage of 30 kV) equipped with a Pegasus analytical complex. Thin foils 3 mm in diameter were prepared using a Fischione 1010 IonMill installation and disks cut at the midradius of a sample and subjected to grinding with a Metaserv 250 machine. The Vickers microhardness (HV) was measured at a load of 1 N using a Micromet 5101 tester equipped with a pyramidal diamond indenter. Tensile tests of flat samples 10.0 mm long, 0.25 mm thick, 1.0 mm wide, and 4.5 mm in gage length, which is located across the midradius of the initial disk, were performed at the Ufa State Aviation Technical University. Before the tests, the sample surface was polished with a diamond paste.

RESULTS

Results of previous studies showed that the hot forging allows the grain size to be refined to 0.5–1 mm. However, the subsequent cooling of the alloy rods in air leads to the decomposition $\beta \rightarrow \beta_1 + \gamma_2$ (at temperatures above T_{ed} that is close to 840 K) and the eutectoid decomposition $\beta_1 \rightarrow \alpha + \gamma_2$ (at temperatures below T_{ed}), where the α phase has the fcc lattice and the γ_2 phase is based on the Cu_9Al_4 intermetallic and has a cubic lattice ($D0_3$) [9–11]. The quenching of the alloys after hot forging prevents the eutectoid decomposition. At the same time, above the eutectoid temperature and temperature of the onset of TMT (M_s) β austenite undergoes two "disorder–order" transitions ($\beta \rightarrow \beta_2(B2) \rightarrow \beta_1(D0_3)$), which ensure the fact that the martensite inherits the long-range atomic order from the initial atomically ordered austenite phase and, therefore, its thermoelasticity [1–6].

According to XRD data, two martensite phases, namely, β' ($18R$) (the parameters of the long-period monoclinic lattice are $a = 0.4450$, $b = 0.5227$, $c = 3.8050$ nm, and $\beta = 91.0°$) and γ_1' ($2H$) (the parameters of orthorhombic lattice are $a = 0.4390$, $b = 0.5190$, and $c = 0.4330$ nm) appear in the quenched β_1 alloy at temperatures below M_s close to 250 K (Fig. 1a and Table 1). It was found that the HPT with 10 revolutions at room temperature causes the deformation-induced TMT with the formation of a mixture of three martensite phases, such as α, β_1', and γ_1' (Fig. 1b). In this case, the found Bragg reflections are substantially broadened (the half-width is to 2 deg) and coincide with intense reflections of these martensite phases. The temperature dependences $\rho(T)$ measured during thermal cycles "cooling–heating" (Fig. 2, curves *1* and *2*) or "heating–cooling" (Fig. 2, curve *3*) demonstrate changes in the shape of TMT hysteresis loops and temperatures of the TMT, which were determined by two tangents method (Table 1). The data agree with XRD data on the phase composition (Fig. 1).

It is of importance to note that the hysteresis of TMT (ΔT) of the HPT-processed alloy increases by more than three times; in this case, all critical temperatures markedly increase.

It follows from the analysis of XRD patterns of the HPT-processed alloy subjected to annealing at 373 and 473 K that the β_1' and γ_1' martensite phases remain

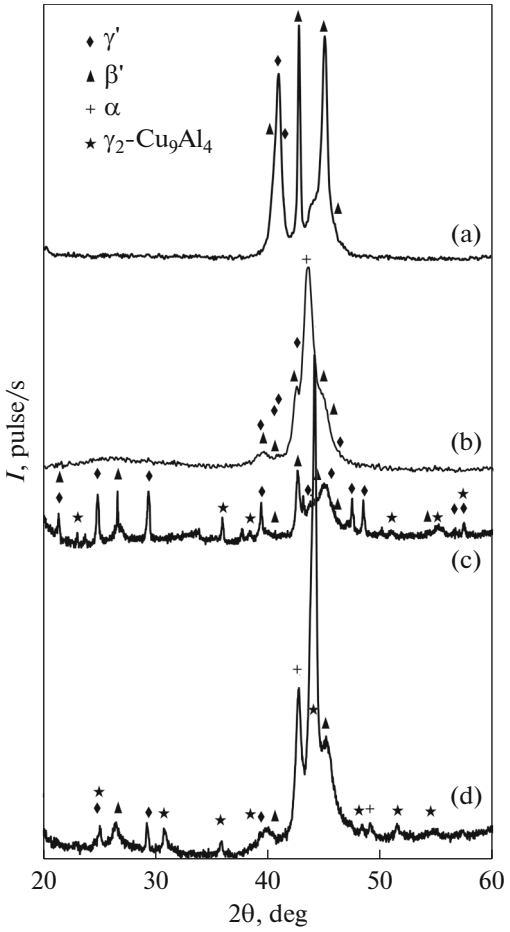

Fig. 1. X-ray diffraction patterns of the Cu–14Al–3Ni alloy subjected to (a) quenching, (b) HPT with 10 revolutions, and HPT and annealing at (c) 373 and (d) 573 K. Measurement temperatures are (a) 200 K and (b–d) room temperature.

and reflections belonging to the γ_2 aging phase appear (see Fig. 1c).

The annealing at the temperatures above A_f, namely, at temperatures of 573–773 K, leads to the eutectoid decomposition of the β_1 austenite into the $(\alpha + \gamma_2)$ phases (see Fig. 1d). The annealing at 873 K causes the decomposition of austenite with the formation of the γ_2 phase. The cooling of the HPT-processed alloy to room temperature accompanied by TMT occurred in the residual β_1 matrix (Figs. 1b, 1d).

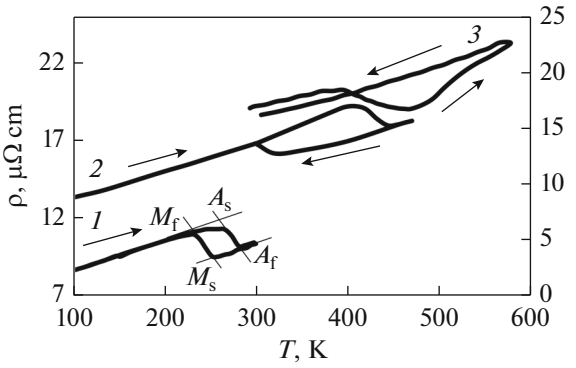

Fig. 2. Temperature dependences $\rho(T)$ of the Cu–14Al–3Ni alloy subjected to different treatments: (*1*) water quenching from 1223 K, measuring cycle 300 K → 90 K → 300 K; (*2*) HPT, measuring cycle 300 K → $T_{L/n}$ → 470 K → 300 K; and (*3*) HPT, measuring cycle 300 K → 573 K → 300 K.

The TEM studies showed that the HPT with increasing number of revolutions from 1 to 10 and, therefore, the increase in the value of deformation of the Cu–14Al–3Ni martensite alloy results in the formation of nanograin structure with ever-increasing homogeneity (Fig. 3); the structure is characterized by ring distribution of reflections in electron diffraction patterns (see Fig. 3).

The quantitative analysis of bright- and dark-field TEM images of the microstructure of alloy subjected to HPT with 10 revolutions shows that the sizes of the most frequently observed randomly oriented structural fragments vary from 10 to 80 nm and in average are equal to 30 nm. It is seen that the coarsest fragments are characterized by the presence of lamellar nanotwins. The processing of electron diffraction patterns shows that the nanocrystalline structure obtained in the alloy mainly comprises the β_1' and γ_1' martensite phases. The ring distribution of reflections indicates the presence of nanosized phases that form the disordered ultrafine-grained (UFG) structure.

The SEM study of the effect of annealing temperature on the microstructure of HPT-processed alloy showed the following. The annealings at 373 and 473 K do not lead to marked size and morphological changes in the UFG martensitic structure resulting from the HPT (Fig. 4a). The growth of globular grains in the

Table 1. Critical temperatures of the start (M_s, A_s) and finish (M_f, A_f) of TMT of the Cu–14Al–3Ni alloy subjected to different treatments (Fig. 2, curves *1*, *2*, *3*)

Treatment	M_s, K	M_f, K	A_s, K	A_f, K	ΔT*, K
Quenching from 1223 K (*1*)	250	230	265	285	35
HPT with 10 revolutions (*2*)	320	300	400	440	110
HPT with 10 revolutions (*3*)	–	–	380	470	–

* $\Delta T = 1/2\{(A_s + A_f) - (M_s + M_f)\}$.

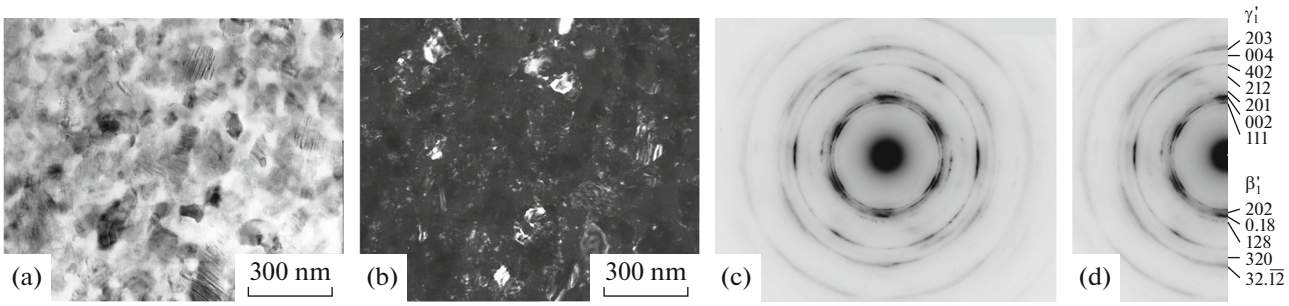

Fig. 3. (a) Bright- and (b) dark-field TEM images of the microstructure of the Cu–14Al–3Ni alloy subjected to repeated quenching from 1273 K and HPT with 10 revolutions and (c, d) associated electron diffraction pattern with key patterns.

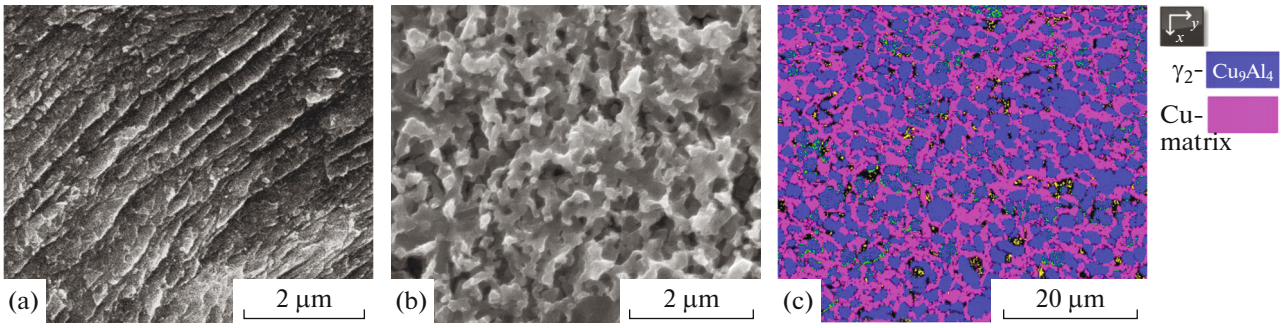

Fig. 4. SEM images of the structure of the Cu–14Al–3Ni alloy subjected to HPT with 10 revolutions and 30-min annealings at (a) 373, (b) 673, and (c) 873 K taken in (a, b) secondary electron and (c) scattered electron diffraction mode for the γ_2-Cu_9Al_4 phase and copper matrix.

alloy is ensured by the annealings at temperatures 573 to 873 K (Figs. 4b, 4c).

The Cu–14Al–3Ni alloy subjected to HPT with 10 revolutions and annealings in the β_1-austenite state was studied by TEM (Fig. 5). It follows from the bright-field TEM images of the microstructure of the annealed alloy that, in accordance with data obtained from electron diffraction patterns, globular nanocrystallites of mainly α and γ_2 phases form in the β_1 matrix and begin to grow (the average size $\langle d_g \rangle$ grains or crystallites is given in Table 2).

Table 2. Average grain size of the Cu–14Al–3Ni alloy subjected to HPT with 10 revolutions and different annealings (according to TEM data)

Alloy treatment	Average grain size $\langle d_g \rangle$, nm
HPT, n = 10 revolutions	30
HPT + 373 K for 30 min	30
HPT + 473 K for 30 min	30
HPT + 573 K for 30 min	100
HPT + 673 K for 30 min	150
HPT + 773 K for 30 min	350
HPT + 873 K for 30 min	400

It is obvious that the heating of reverted β_1 austenite at 573 K ensures the complex reaction of the recrystallization process and eutectoid ($\alpha + \gamma_2$) decomposition. In this case, mainly small grains–crystallites, at the background of coarser recrystallized grains, are mark out by intense deformation contrast and remain almost unchanged in size. In average, $\langle d_g \rangle$ is close to 100 nm (see Fig. 5a). It should be noted that, in this case, the reflections in the electron diffraction patterns are characterized by continuous ring distribution (Fig. 5e). The observed peculiarities of structure orientation and morphology indicate the presence of low- and high-angle boundaries inherited after HPT by both reverted austenite and then martensite phases that are present in the residual β_1 phase already at room temperature after TMT.

According to TEM data, the increase in the annealing temperature to 673 K leads to the almost complete primary recrystallization of the β_1 austenite and formation of ($\beta_1 + \alpha + \gamma_2$) triplex structure in the composition of uniform UFG austenite with the increased $\langle d_g \rangle$ close to 150 nm. Grains–crystallites remain rounded and their boundaries remain curved; the high density of defects still remains in the structure (Fig. 5b). The ring character of already less uniform distribution of point defects in the electron diffraction patterns of the HPT-processed alloy annealed at 673–

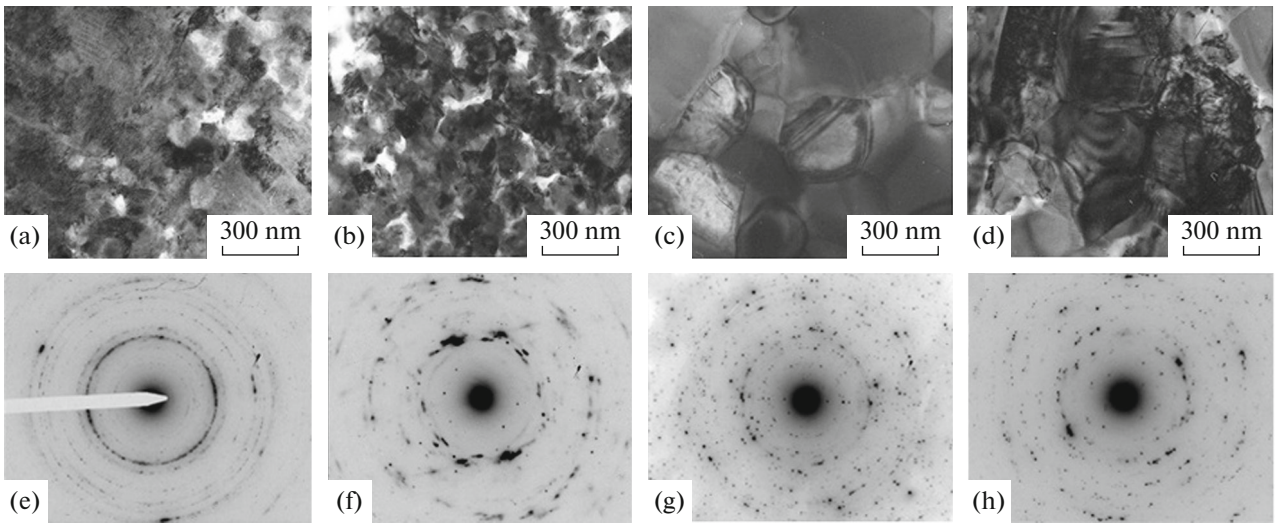

Fig. 5. Bright-field TEM images of the UFG structure and corresponding electron diffraction patterns of the Cu–14Al–3Ni alloy subjected to HPT with 10 revolutions and isochronous annealings (for 30 min) at (a, e) 573, (b, f) 673, (c, g) 773, and (d, h) 873 K.

873 K indicates the presence of a great amount of random orientations of globular grains–crystallites arisen in the alloy (see Figs. 5f–5h). At the higher isochronous annealing temperature, namely, at 773 K, the more active coarsening of α- and γ_2-phase globules with $\langle d_3 \rangle$ close to 350 nm, which are formed in the β_1 austenite, takes place (Fig. 5c). After annealing at 873 K, $\langle d_3 \rangle$ of the β_1 and γ_2 phases is close to 400 nm (Table 2, Fig. 4c). In this case, images of grain-crystallite boundaries of the (β_1 + γ_2) duplex structure become clearer, and a twin contrast is observed in the martensite (see Fig. 5d). "Sharp" point reflections in the electron diffraction patterns indicate the substantial relaxation of internal stresses and interfacial distortions in the UFG structure formed by precipitated phases and martensite.

Thus, as a result of performed studies, it was found that the isochronous annealings beginning from the temperatures above A_f in a range of 473 to 873 K lead to the recrystallization of β_1 ($D0_3$) austenite in the HPT-processed Cu–14Al–3Ni alloy and formation of sufficiently uniform UFG structures; in this case, the grain size increases from 30 to 400 nm, respectively (Table 2).

In all cases, beginning from the low-temperature (below M_s) annealing at 373–473 K, at which the HPT-processed alloy underwent partial martensite decomposition accompanied by the precipitation of fine γ_2-phase particles, reflections of the phase are present in X-ray and electron diffraction patterns taken, namely, after annealings at 573–773 K as a result of eutectoid ($\alpha + \gamma_2$) decomposition of austenite and at 873 K as a result of the proeutectoid (β_1 + γ_2) decomposition. When the matrix β_1-austenite phase remains during annealing (this takes place in the case of used conditions), the TMT occurs during subsequent cooling.

The microhardness *HV* measured at the midradius of disks of the HPT-processed Cu–14Al–3Ni alloy is gives in Fig. 6 as a function of the annealing temperature. After annealing at 573 K, the HPT-processed Cu–14Al–3Ni alloy exhibits the maximum values of microhardness *HV*, up to 5850 MPa after single quenching from 1223 K and 5550 MPa after repeated quenching from 1273 K. The repeated quenching ensures the better homogenization of the alloy solid solution as compared to that reached after single quenching and leads to the slightly lower values of microhardness (*HV*). It should be noted that, after HPT, the microhardness increases by 1000 MPa as compared to the hardness for the initial quenched state. The trend towards the increase in the micro-

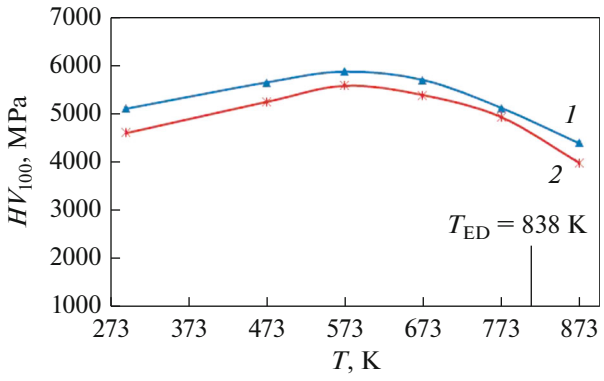

Fig. 6. Dependences of microhardness *HV* of the Cu–14Al–3Ni alloy on the annealing temperature for 30 min: (*1*) quenching from 1223 K and (*2*) quenching from 1273 K.

Table 3. Results of tensile tests of the Cu–14Al–3Ni alloy after different deformation and heat treatments

No.	Treatment	σ_m, MPa	σ_u, MPa	ε_m, %	δ, %
1	Quenching from 1223 K	160	620	2	7
2	Quenching from 1273 K	60	400	2	11
3	HPT with 10 rev., (293 K)	–	820	–	4
4	HPT with 10 rev., (423 K)	–	1450	2	12
5	HPT + 573 K for 30 min	120	450	2	6
6	HPT + 773 K for 30 min	50	320	3	8
7	HPT + 1073 K for 10 s	250	900	5	13

hardness of the HPT-processed alloy remains also after used annealings.

Table 3 gives the results of tensile tests of the Cu–14Al–3Ni alloy at room temperature. The tests showed that the quenched CG alloy exhibits the ultimate strength (σ_u) equal to 620 MPa, critical strength of martensitic shift (σ_m) equal to 160 MPa with a pseudoelastic phase yield (ε_m) of to 2%, and a relative elongation to failure (δ) of 7%. The repeated quenching of the alloy leads to the increase in δ to 11% at a slight softening at the expense of the formation of fine-grained (FG) state. The value of δ of the strengthened UFG alloy subjected to HPT at room temperature decreases to 4%, and the failure is brittle and occurs without the necking. In this case, in contrast to the CG and FG alloy (for which $\varepsilon_m = 2\%$), the phase yield plateau is not fixed. The increase in the HPT temperature to 423 K (by 130 K above room temperature) leads to the unusually high deformation-induced strengthening of the Cu–14Al–3Ni alloy and, at the same time, to the substantial increase in δ that is 12%. The highest mechanical characteristics were reached for the HPT-processed alloy. In particular, the yield stress is 1400 MPa, and the ultimate strength is 1450 MPa at the high relative elongation to failure ($\delta = 12\%$). The substantial changes in the mechanical behavior of the alloy were observed after HPT with 10 revolutions at annealing temperatures 573 to 1073 K and annealing times 10 s to 30 min, which result in the formation of the UFG structure (see Table 3).

Studies of fractures of samples subjected to tensile tests show that the rapture of initial hot-forged quenched coarse-grained alloy is brittle; the spalling primary occurs along grain boundaries and boundaries of large martensite crystal packets (Fig. 7a). The nanosized grain–subgrain structure of alloy subjected to HPT with 10 revolutions exhibits changing in the fracture type and character of rupture of samples (Fig. 7b).

The fracture demonstrates numerous strain localization centers with formed small planar pits and, therefore, low tearing off ridges. This is typical of ductile intragranular low-energy rupture mechanism. The average pit size is 2–5 μm, which exceeds the size of UFG structure elements of the HPT-processed alloy by two orders of magnitude. This circumstance indicates the specific intercrystalline failure mechanism of the alloy; the rapture occurs mainly along high-angle boundaries of the UFG structure. However, the size of cellular fragments (pits) of tearing off upon brittle-ductile failure becomes lower by two orders of magnitude as compared to sizes of grains and brittle spall areas in the initial CG alloy; this finally determines the high plasticity of the UDG alloy.

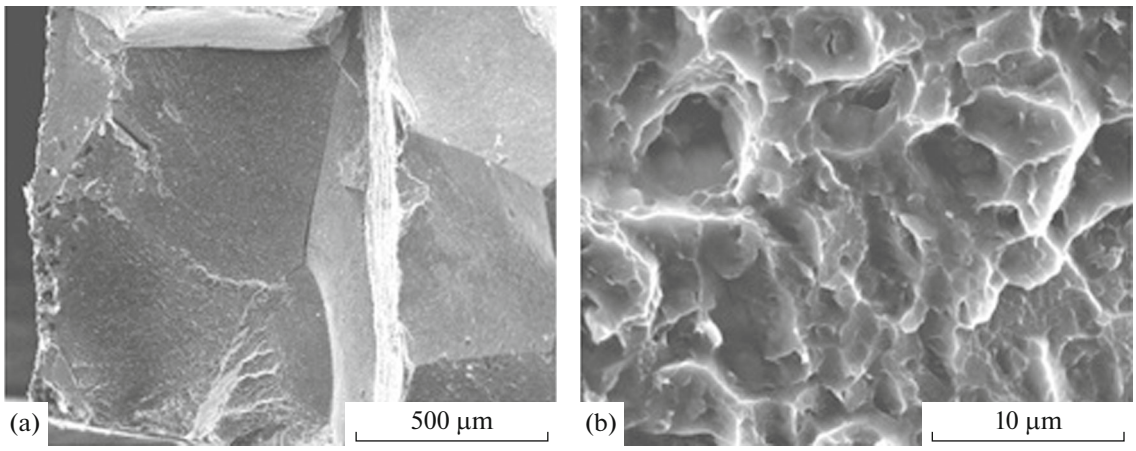

Fig. 7. SEM images of fractures of (a) hot-forged quenched Cu–14Al–3Ni alloy and (b) the alloy subjected to HPT with 10 revolutions.

DISCUSSION

As was previously found [8–14], under certain conditions, the MPD of eutectoid SME Cu–Al–Ni alloys is the efficient method for radical refining their grain structure and, therefore, plasticization. It is shown in this study that the HPT with high plastic deformations ensures the mechanically induced TMT in the metastable Cu–14Al–3Ni austenitic alloy and simultaneous formation of uniform nanosized UFG structure. It is characterized by high hardness, strength, and high stability of martensite phases with respect to the reverse TMT during heating. The critical temperatures of TMT of the alloy subjected to HPT with 10 revolutions increase; namely, M_s and M_f increase by 70 K, whereas A_s and A_f increase by 150 K. It is possible to conclude that, when measuring $\rho(T)$, the increase in the temperatures of reverse TMT during heating and subsequent cooling is due, according to phase analysis data, mainly to the effect of heterogeneous precipitation (at martensite boundaries and subboundaries) of γ_2 phase, which is responsible for both size stabilization of martensite grains–crystallites and chemical stabilization due to the their depletion of aluminum and enrichment in copper (by 1–2 at % judging from the data on M_s–A_f). In this case, the available concentration dependence of the temperatures of TMT on the contents of copper and aluminum allows us to determine the chemical composition of the β_1 matrix of the Cu–Al–Ni alloys.

At the same time, in the case of complex analysis by XRD, TEM, and SEM, a number of peculiarities of the fine structure and phase composition of the HPT-processed alloy subjected to above isothermal annealings were revealed. It was found that, at relatively low annealing temperatures (373–473 K), the martensite phases remain in the HPT-processed alloy. In this case, the appearance of reflections belonging to the γ_2 aging phase and disappearance of reflections belonging to the α' martensite phases, which is likely to transform to the β' martensite, takes place. On the contrary, the annealing at the higher temperatures, above A_f, leads to the disappearance of martensite phases as a result of reverse TMT in the UFG austenite. In this case, during annealing at temperature below T_{ed}, the eutectoid ($\alpha + \gamma_2$) decomposition of the austenite phase into the globular UFG triplex structure occurs; during annealing above T_{ed}, the precipitation of the γ_2 phase occurs with the formation of the ($\beta_1 + \gamma_2$) duplex structure. During cooling to room temperature and under deformation, the TMT is possible.

In this case, it is of importance that the post-deformation annealing of the HPT-processed alloy forms structures that can undergo the SME and phase ductility over a wide range of martensite yield stresses σ_m of 50 to 450 MPa (Table 3). In whole, the martensitic deformation, including the formation of martensite crystals, detwinning, and their reorientation along applied forces make the marked contribution to the ability of the alloy to plastic deformation. For example, the Cu–14Al–3Ni alloy subjected to HPT with 10 revolutions and short-term annealing at 1073 K for 10 s exhibits the relatively high δ (13%) that is due to the combination of phase yield (ε_m) and prolonged stage of subsequent plastic deformation of martensite (Table 3). When reaching the value $\sigma_u = 900$ MPa, the strain localization and development of a small necking take place [1].

CONCLUSIONS

(1) It was found that the megaplastic deformation of the metastable Cu–14Al–3Ni austenite alloy by torsion under a high pressure of 6 GPa (with a number of revolutions of 1 to 10) leads to the formation of deformation-induced ultrafine-grained structure of martensite, which is responsible for its high both hardness and strength properties.

(2) It was shown that the subsequent short-term annealing ensures retaining the UFG structure and strengthening of the alloy. The highest strength (σ_u is to 1400 MPa) and improved plastic properties (δ = 12–13%) are obtained for the UFG martensite alloys in using short-term annealing at 1073 K for 10 s after HPT with 10 revolutions or at the expense of the increase in the HPT temperature to 423 K (150°C).

(3) It was found that, during annealing at the temperature below M_s, which initiates the heterogeneous (proeutectoid) decomposition of martensite in the HPT-processed alloy and precipitation of aluminum-enriched γ_2 phase, the grain size, phase composition, and substructure of martensite retain. However, the depletion of martensite of aluminum by 1–2 at % causes the stabilization of martensite and marked increase in the critical temperatures of TMT (by 70–150 K).

(4) The annealing of the alloy in the austenitic state above the A_f temperature in a range of 570–840 K leads to the primary recrystallization accompanied by the heterogeneous eutectoid ($\alpha + \gamma_2$) decomposition of β_1 austenite with retaining the uniform UFG ($\beta_1 + \alpha + \gamma_2$) triplex structure. Above T_{ed} close to 840 K, the ($\beta_1 + \gamma_2$) duplex structure forms when the γ_2-nanophase precipitates; in this case, the high microhardness of the alloy after TMT during cooling to room temperature is reached.

(5) According to results of fractography, the alloy in the UFG state is characterized by brittle-ductile failure with high dispersion of pits of tearing off along high-angle boundaries of ensembles of nanograins integrated by low-angle misorientations.

ACKNOWLEDGMENTS

We thank Ufa State Aviation Technical University for performed mechanical tests.

FUNDING

The study was performed in terms of state assignment no. AAAA-A18-118020190116-6 (Struktura) of the joint laboratory of the Institute of Metal Physics, Ural Branch, Russian Academy of Sciences and Ural Federal University.

REFERENCES

1. Kh. Varlimont and L. Dilei, *Martensite Transformations in Alloys Based on Copper, Silver, and Gold* (Nauka, Moscow, 1980) [in Russian].
2. V. A. Likhachev, S. L. Kuz'min, and Z. P. Kamentseva, *Shape Memory Alloys* (LSU, Leningrad, 1987) [in Russian].
3. K. Oksuka, C. M. Wayman, T. Saburi, T. Tadaki, T. Maki; Y. Suzuki, J. Van Humbeeck, R. Stalmans, K. Uchino, M. Irie, K. N. Melton, I. Ohkata, and S. Miyazaki, *Shape Memory Materials*, Ed. by K. Otsuka and C. M. Wayman (Cambridge, 1999).
4. V. N. Khachin, V. G. Pushin, and V. V. Kondrat'ev, *Titanium Nickelide. Structure and Properties* (Nauka, Moscow, 1992) [in Russian].
5. V. G. Pushin, V. V. Kondrat'ev, and V. N. Khachin, *Pretransition Phenomena and Martensite Transformations* (UrBr RAS, Yekaterinburg, 1998) [in Russian].
6. R. Dasgupta, "A look into Cu–based shape memory alloys: Present Scenario and future prospects," J. Mater. Res. **29**, No. 16, 1681–1698 (2014).
7. P. Sedlak, H. Seiner, M. Landa, V. Novák, P. Šittner, and L. I. Manosa, "Elastic constants of bcc austenite and 2H orthorhombic martensite in CuAlNi shape memory alloy," Acta Mater. **53**, 3643–3661 (2005).
8. G. A. Lopez, I. Lopez-Ferreno, A. R. Kilmametov, T. Breczewski, B. B. Straumal, B. Baretzky, M. L. No, and J. San Juan, "Severe plastic deformation on powder metallurgy Cu–Al–Ni shape memory alloys," Mater. Today: Proc. **2**, 747–750 (2015).
9. A. E. Svirid, V. G. Pushin, N. N. Kuranova, A. V. Luk'yanov, A. V. Pushin, A. N. Uksusnikov, and Y. M. Ustyugov, "The structure–phase transformations and mechanical properties of the shape memory effect alloys based on the system Cu–Al–Ni," Materials Today: Proc. **4**, 4758–4762 (2017).
10. A. E. Svirid, N. N. Kuranova, A. V. Luk'yanov, V. V. Makarov, N. V. Nikolaeva, V. G. Pushin, and A. N. Uksusnikov, "Influence of thermomechanical treatment on structural-phase transformations and mechanical properties of the Cu–Al–Ni shape-memory alloys," Russ. Phys. J. **61**, 1681–1686 (2018).
11. A. V. Lukyanov, V. G. Pushin, N. N. Kuranova, A. E. Svirid, A. N. Uksusnikov, Yu. M. Ustyugov, and D. V. Gunderov, "Effect of the thermomechanical treatment on structural and phase transformations in Cu–14Al–3Ni shape memory alloy subjected to high-pressure torsion," Phys. Met. Metallogr. **119**, No. 4, 374–382 (2018).
12. A. E. Svirid, A. V. Luk'yanov, V. G. Pushin, E. S. Belosludtseva, N. N. Kuranova, and A. V. Pushin, "Effect of the temperature of isothermal upsetting on the structure and the properties of the shape memory Cu–14 wt % Al–4 wt % Ni alloy," Phys. Met. Metallogr. **120**, 1159–1165 (2019).
13. A. E. Svirid, V. G. Pushin, N. N. Kuranova, V. V. Makarov, A. V. Pushin, A. N. Uksusnikov, and A. V. Luk'yanov, "Application of isothermal upset for megaplastic deformation of Cu–Al–Ni β alloys," Tech. Phys. **90**, 1044–1055 (2020).
14. A. E. Svirid, A. V. Luk'yanov, V. V. Makarov, V. G. Pushin, and A. N. Uksusnikov, "Influence of doping with aluminum on the structure, phase transformations and properties of Cu–Al–Ni alloys with shape memory effect," Chelyabinskii Fiz.-Mat. Zh. **4**, 108–117 (2019).
15. A. Pelosin and A. Riviere, "Structural and mechanical spectroscopy study of the β_1' martensite decomposition in Cu – 12% Al – 3% Ni (wt %) alloy," J. Alloys Compd. **268**, 166–172 (1998).
16. F. Dagdelen, T. Gokhan, A. Aydogdu, Y. Aydogdu, and O. Adiguzel, "Effect of thermal treatments on transformation behavior in shape memory Cu–Al–Ni alloys," Mater. Lett. **57**, 1079–1085 (2003).
17. Z. Li, Z. Y. Pan, N. Tang, Y. B. Jiang, N. Liu, M. Fang, and F. Zheng, "Cu–Al–Ni–Mn shape memory alloy processed by mechanical alloying and powder metallurgy," Mater. Sci. Eng., A **417**, 225–229 (2006).
18. N. Suresh and U. Ramamurty, "Aging response and its effect on the functional properties of Cu–Al–Ni shape memory alloys," J. Alloys Compd. **449**, 113–118 (2008).
19. R. D. Dar, H. Yan, and Y. Chen, "Grain boundary engineering of Co–Ni–Al, Cu–Zn–Al, and Cu–Al–Ni shape memory alloys by intergranular precipitation of a ductile solid solution phase," Scr. Mater. **115**, 113–117 (2016).
20. P. La Roca, L. Isola, Ph. Vermaut, and J. Malarria, "Relationship between grain size and thermal hysteresis of martensitic transformations in Cu-based shape memory alloys," Scr. Mater. **135**, 5–9 (2017).
21. X. Zhang, X. Zhao, F. Wang, L. Qingsuo, and Q. Wang, "Microstructure, mechanical properties and shape memory effect of Cu–Hf–Al–Ni alloys," Mater. Sci. Technol. **34**, No. 12, 1497–1501 (2018).

Translated by N. Kolchugina